NOAA Technical Report NESDIS 128

Influence of the ozone and water vapor on the GOES Aerosol and Smoke Product (GASP) retrieval

Washington, D.C.
May 2008

U.S. DEPARTMENT OF COMMERCE
National Oceanic and Atmospheric Administration
National Environmental Satellite, Data, and Information Service

NOAA TECHNICAL REPORTS

National Environmental Satellite, Data, and Information Service

The National Environmental Satellite, Data, and Information Service (NESDIS) manages the Nation's civil Earth-observing satellite systems, as well as global national data bases for meteorology, oceanography, geophysics, and solar-terrestrial sciences. From these sources, it develops and disseminates environmental data and information products critical to the protection of life and property, national defense, the national economy, energy development and distribution, global food supplies, and the development of natural resources.

Publication in the NOAA Technical Report series does not preclude later publication in scientific journals in expanded or modified form. The NESDIS series of NOAA Technical Reports is a continuation of the former NESS and EDIS series of NOAA Technical Reports and the NESC and EDS series of Environmental Science Services Administration (ESSA) Technical Reports.

An electronic copy of this report may be obtained at
http://www.orbit.nesdis.noaa.gov/smcd/spb/ozone/pubs_docs.html

A limited number of copies of earlier reports are available by contacting Susan Devine, NOAA/NESDIS, E/RA3, 5200 Auth Road, Room 701, Camp Springs, Maryland 20746, (301) 763-8127 x136. Copies can also be ordered from the National Technical Information Service (NTIS), U.S. Department of Commerce, Sills Bldg., 5285 Port Royal Road, Springfield, VA 22161, (703) 487-4650 (prices on request for paper copies or microfiche, please refer to PB number when ordering). A partial listing of more recent reports appears below:

NESDIS 99   The Use of Water Vapor for Detecting Environments that Lead to Convectively Produced Heavy Precipitation and Flash Floods. Rod Scofield, Gilberto Vicente, and Mike Hodges, September 2000.

NESDIS 100   The Resolving Power of a Single Exact-Repeat Altimetric Satellite or a Coordinated Constellation of Satellites: The Definitive Answer and Data Compression. Chang-Kou Tai, April 2001.

NESDIS 101   Evolution of the Weather Satellite Program in the U.S. Department of Commerce - A Brief Outline. P. Krishna Rao, July 2001.

NESDIS 102   NOAA Operational Sounding Products From Advanced-TOVS Polar Orbiting Environmental Satellites. Anthony L. Reale, August 2001.

NESDIS 103   GOES-11 Imager and Sounder Radiance and Product Validations for the GOES-11 Science Test. Jaime M. Daniels and Timothy J. Schmit, August 2001.

NESDIS 104   Summary of the NOAA/NESDIS Workshop on Development of a Coordinated Coral Reef Research and Monitoring Program. Jill E. Meyer and H. Lee Dantzler, August 2001.

NESDIS 105   Validation of SSM/I and AMSU Derived Tropical Rainfall Potential (TRaP) During the 2001 Atlantic Hurricane Season. Ralph Ferraro, Paul Pellegrino, Sheldon Kusselson, Michael Turk, and Stan Kidder, August 2002.

NESDIS 106   Calibration of the Advanced Microwave Sounding Unit-A Radiometers for NOAA-N and NOAA-N=. Tsan Mo, September 2002.

NOAA Technical Report NESDIS 128

Influence of the ozone and water vapor on the GOES Aerosol and Smoke Product (GASP) retrieval

Hai Zhang[1], Raymond Hoff[1], Kevin McCann[1], Pubu Ciren[2], Shobha Kondragunta[3], and Ana Prados[1]

1. University of Maryland Baltimore County
   Joint Center for Earth Systems Technology
   5523 Research Park Drive
   Baltimore, MD 21228

2. Perot Systems Government Services
   5200 Auth Road
   Camp Springs, MD 20746

3. NOAA/NESDIS/STAR
   5200 Auth Road
   Camp Springs, MD 20746

Washington, DC
May 2008

TABLE OF CONTENTS

FIGURES

ABSTRACT

The GOES Aerosol and Smoke Product (GASP) is an aerosol optical depth (AOD) retrieval product from GOES imagery, providing near-real time AOD for the United States region at 30-minute intervals. One potential source of error in its retrieval algorithm is that it assumes a constant total column water vapor and ozone when calculating gaseous absorption. The purpose of this work is to estimate the errors introduced by the water vapor and ozone content in the GASP retrieval. GASP retrieval algorithm runs were undertaken in both simulated and real data cases. We found relatively small errors due to the gaseous absorption. The retrieved AODs are more sensitive to water vapor and ozone variations in the early morning and late afternoon due to larger air mass. A correction algorithm was developed, but it does not show much improvement, which concludes that the current GASP algorithm which uses fixed values of water vapor and ozone is satisfactory.

1. INTRODUCTION

Aerosols not only play an important role in the climate system through perturbing the radiation budget (*Herman and Browning* 1975; *Charlson et al.* 1991; *Haywood et al.* 1999) and indirect cloud effects (*Platnick and Twomey* 1994; *Kaufman et al.* 2002), but also are deeply involved in affecting air quality. Since poor air quality is very harmful to human health, recent efforts have been made to track and forecast pollution using the satellite measurement of aerosols (*Al-Saadi et al.* 2005; *Engel-Cox et al.* 2004; *Hoff et al.* 2005). In order to do this, it is very important to have aerosol information at high temporal and spatial resolution.

The GOES Aerosol and Smoke Product (GASP) is an aerosol optical depth (AOD) product from the GOES imager (*Knapp et al.* 2002, 2005; *Prados et al.* 2007). Currently, GASP uses GOES-12 visible channel data for the AOD retrieval, and channels 2 and 4 for the cloud masking algorithm. It runs in near-real time at NOAA's National Environmental Satellite Data and Information Service (NESDIS) with 30-minute interval and 4km×4km spatial resolution (http://www.ssd.noaa.gov/PS/FIRE/GASP/gasp.html). A distinguishing feature of GASP is its high temporal resolution compared to other AOD retrieval products, such as MODIS, which has only two retrievals per day (*Kaufman et al.* 1997; *Remer et al.* 2005). This feature enables the diurnal variations of AOD (day time) and the transport of aerosols to be monitored.

GASP uses a look-up table (LUT) generated from Second Simulation of the Satellite Signal in the Solar Spectrum (6S) radiative transfer model (*Vermote et al.* 1997) to derive AOD from the composite image. GASP uses a 21 day composite clear sky background for reference from which current day radiances in the visible channel are compared. The radiance difference is converted to AOD after correction of clear sky gaseous absorption and correction for satellite-sun geometries as a function of time of day. The primary gaseous absorption is from water vapor and ozone (Figure 1), and the GASP assumes a constant column water vapor and ozone from the climatological data when building the LUT. Since water vapor and ozone have significant spatial and temporal variations, this assumption could be a source of errors in the retrieval. *Knapp et al.* (2002) gave a brief analysis on this uncertainty for GOES-8 for South America region, and they concluded that the AOD uncertainty resulting from uncertainty in column water vapor and ozone is less than 0.01.

The purpose of this work is to provide a detailed analysis of the errors due to this assumption for GOES-12 over the United States region. The tests are performed in both simulated cases and real data cases. We generate reflectance using random values of column water vapor and ozone, and run the GASP retrievals on them. The uncertainties are analyzed for different geometries and surface reflectance. In real data case, we run the retrieval algorithm with LUTs generated with different column water vapor and ozone. At last, we investigate the possible improvements of the retrieval using a correction algorithm.

2. STATISTICS OF COLUMN WATER VAPOR AND OZONE

The statistics of column water vapor and ozone over the continental US are obtained based on the analysis data acquired from National Center for Environmental Prediction (NCEP, NAM (Eta) Data Assimilation System (EDAS), Total Ozone Analysis using SBUV/2 and TOVS) and ground ozone observational data from World Ozone and Ultraviolet Radiation Data Centre (WOUDC). The range of column water vapor for the whole dataset is from 0 to 6 $g\,cm^{-2}$, the average is 1.99 $g\,cm^{-2}$, and the standard deviation is 1.34 $g\,cm^{-2}$. The average column water vapor changes from 1.23 $g\,cm^{-2}$ in winter to 3.02 $g\,cm^{-2}$ in summer. The diurnal variation of column water vapor ranges from 0.55 $g\,cm^{-2}$ in winter to 0.73 $g\,cm^{-2}$ in summer with an average of 0.66 $g\,cm^{-2}$ over the whole year.
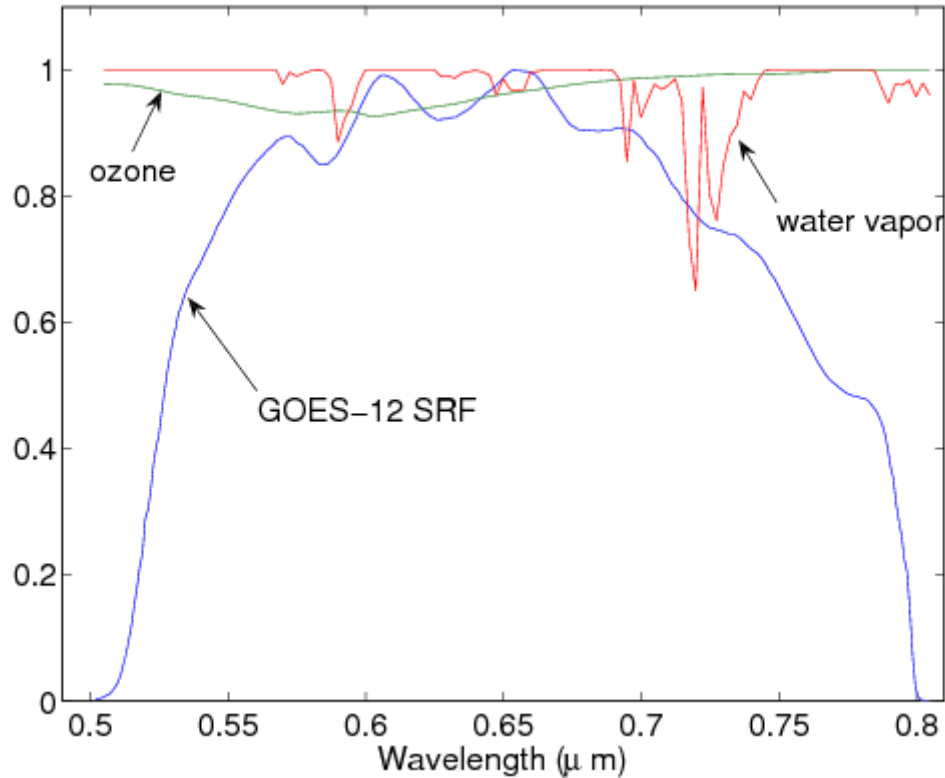
Figure 1: GOES-12 spectral response function (SRF) overlaid with spectral transmittance of ozone and water vapor.

The range of the ozone column is from 220 to 450 DU, the average is 303 DU, and the standard deviation is 37 DU. The column ozone is smallest in fall (SON), and largest in spring (MAM) with the mean value varying from 284.7 DU to 324.7 DU. The average diurnal variation of column ozone is about 30 DU. GASP uses fixed column water vapor value 1.424 g cm^{-2}, and column ozone value 344 DU for generating LUT.

3. GASP ALGORITHM

The GASP AOD retrieval algorithm involves three steps: compilation of the background composite, retrieval of the surface reflectance, and retrieval of the aerosol optical depth (*Knapp et al.* 2002).

In the first step, a clear sky background reflectance for each timestep with 30-minute interval during sun-lit time is generated. In order to avoid the contamination from the cloud shadows, the second darkest point over the past 21 days for each pixel is selected. Besides the contribution from the surface reflectance, the clear sky background also includes atmospheric effects such as molecular scattering, aerosol extinction and gaseous absorption. These effects are removed in the second step through atmospheric correction in order to obtain the surface reflectance.

In the second step, the satellite detected counts for the clear sky background are first converted to reflectance ρ_{sat} (*Knapp and Vonder Haar* 2000). Then, the atmospheric effect is removed through the inversion of the background reflectance to obtain an estimate of the surface reflectance. In this procedure, the background AOD is assumed to be 0.02 to represent the remaining aerosol scattering.

2

In the third step, the reflectance at TOA detected at the current timestep is inverted to retrieve AOD through the use of surface reflectance obtained in the second step. The AOD retrieved is for wavelength 550nm since the AOD in this wavelength is used in 6S for generating the LUT.

After the retrieval, a screening process is performed to remove cloud pixels and pixels with low AOD quality (*Prados et al.* 2007). Besides cloud screening from channel 2 and 4, a pixel is screened if it satisfies one of the following criteria: the retrieved AOD is greater than 2.0; the retrieved surface reflectance is less than 0.005 or greater than 0.15; the standard deviation is greater than 0.2 over a 3×3 pixel box containing the central pixel.

4. SENSITIVITY TESTS

In this section, we perform sensitivity tests for both the simulated cases and for the cases using real data.

4.1. SIMULATED CASES

The sensitivity tests are made by generating 1000 random column water vapor and column ozone with Gausian distribution, and the means and the standard deviations are from the previous section: mean water vapor is 1.99 g cm^{-2}, water vapor standard deviation is 1.34 g cm^{-2}, mean column ozone is 303 DU, ozone standard deviation is 37 DU. These random numbers are then feed to 6S model to produce reflectance at the top of atmosphere with difference geometries and surface reflectance. Finally, retrievals for the surface reflection and AOD are performed using the GASP algorithm.

In the cases for the surface reflection retrievals, the 1000 random cases are generated with 0.02 AOD, and the results are shown in Figure 2 and Figure 3. Both the bias and the standard deviation are both smaller than 10%.

The biases of the AOD retrievals with zero surface reflectance are shown in Figure 4. Positive biases are introduced due to the difference between the mean water vapor and ozone and the assumed values. The bias does not change much as the relative azimuth angle varies, and they increase with increasing solar zenith angle and satellite zenith angle. It is generally smaller than 10% if the solar zenith angle is smaller than 80˚, the satellite zenith angle is smaller than 70˚ and the AOD is less than 1. It is large when both solar and satellite angle are large. The bias also increases nonlinearly with AOD which has more rapid increase when AOD changes from 1.0 to 1.5. The standard deviations of the AOD retrievals for zero surface reflectance are shown in Figure 5. For zero surface reflectance with satellite zenith angle at 30˚, the standard deviation are below 3 percent for the AOD smaller than 1.0 if the solar zenith angle is below 70˚. However, they are much larger at about 10% if the solar zenith angle is about 80˚. For all the satellite and solar zenith angles, the bias and the standard deviation do not change much with different relative azimuth angles.

Figure 6 shows the standard deviation of the retrievals as a function of surface reflectance for 1.0 AOD. The uncertainties are observed to increase with increasing surface reflectance. At 0.1 surface reflectance, the standard deviations are about 5% for small solar and satellite zenith angles, while at 0.15 surface reflectance, they are between 10% and 20%.
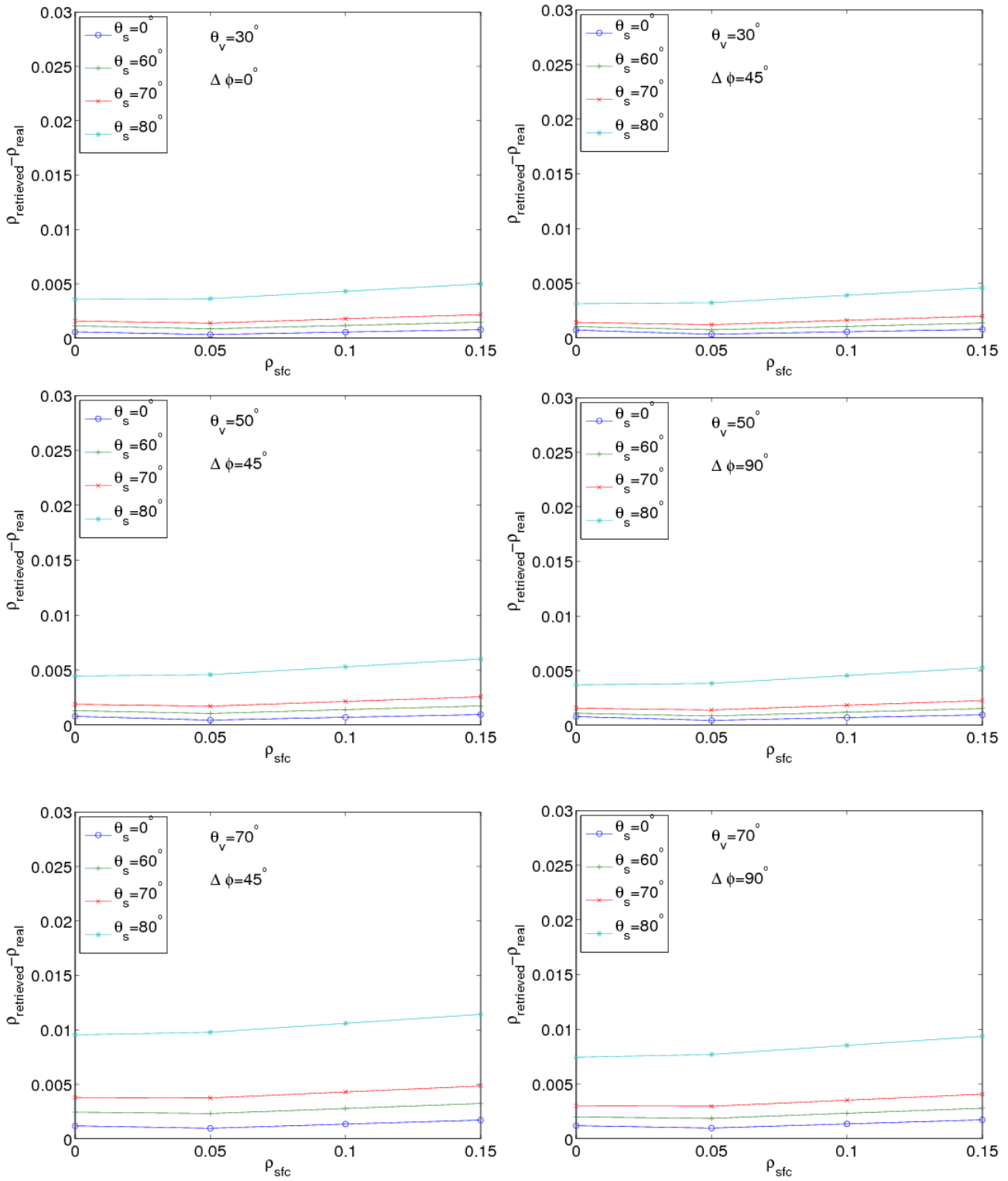
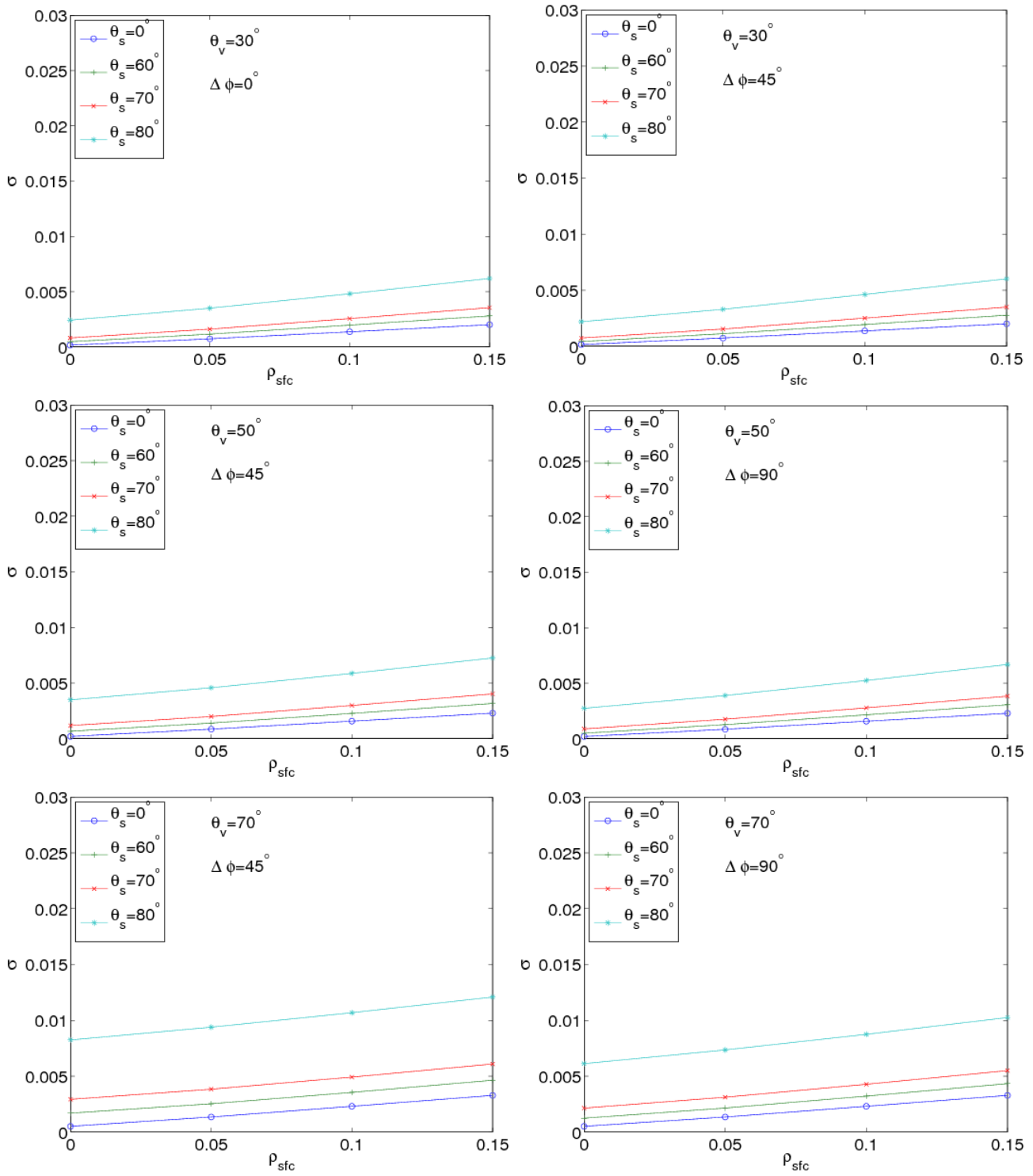**Figure 2: Difference between the retrieved surface reflectance and real surface reflectance**

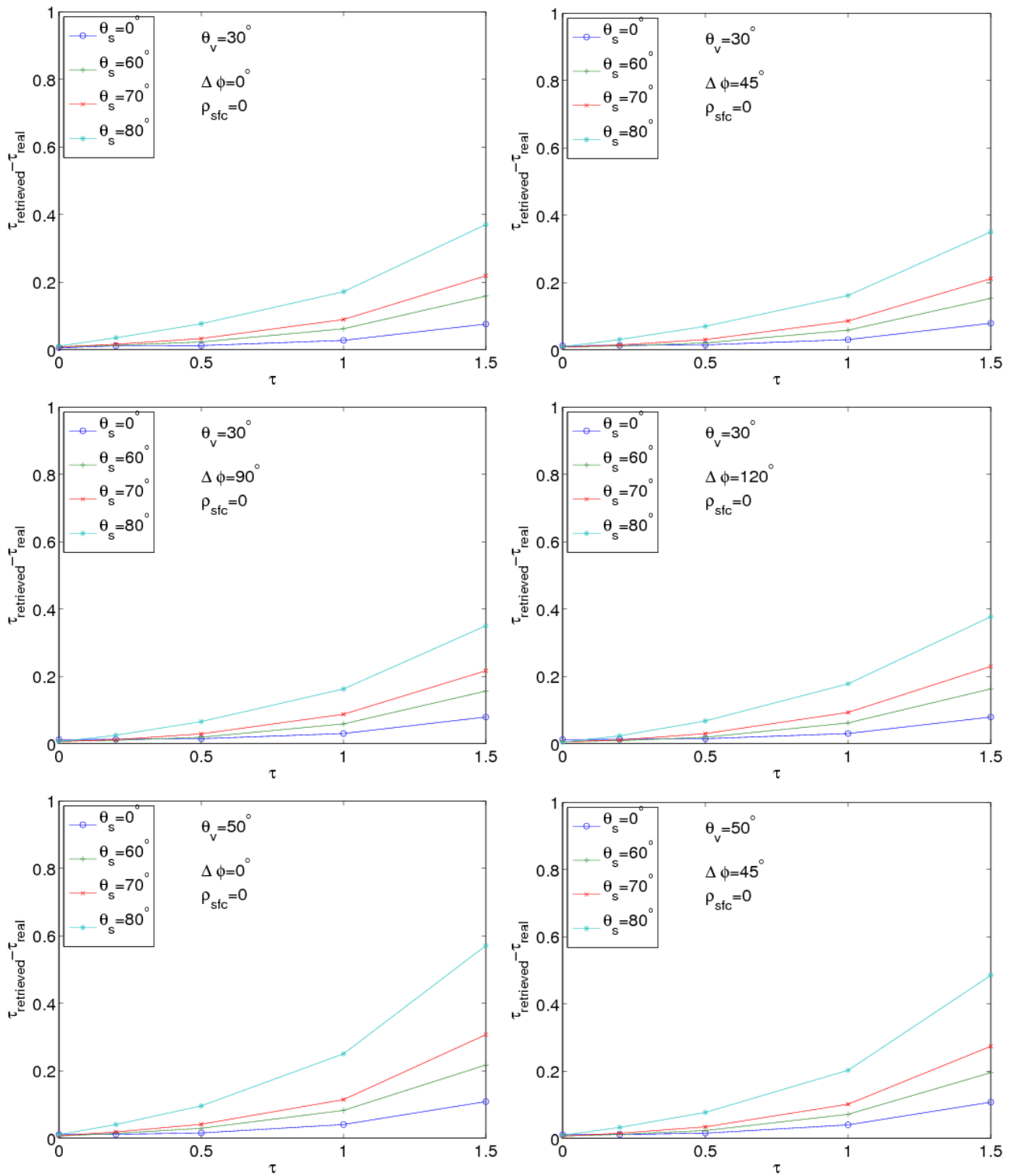**Figure 3: Standard deviation of the retrieved surface reflectance.**

Figure 4: Difference between the retrieved AOD and real AOD for zero surface reflections.
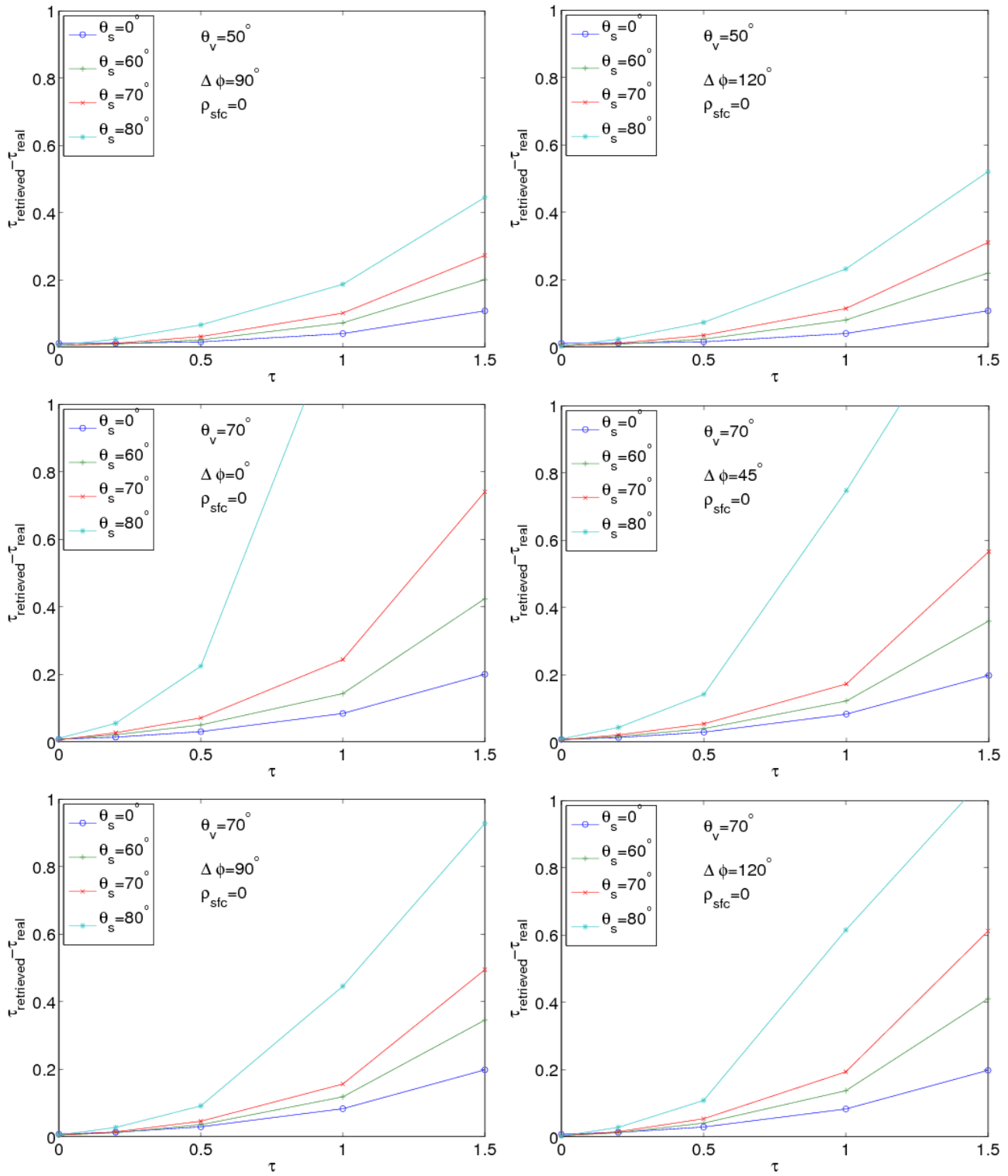
Figure 4: Difference between the retrieved AOD and real AOD for zero surface reflections (cont'd).
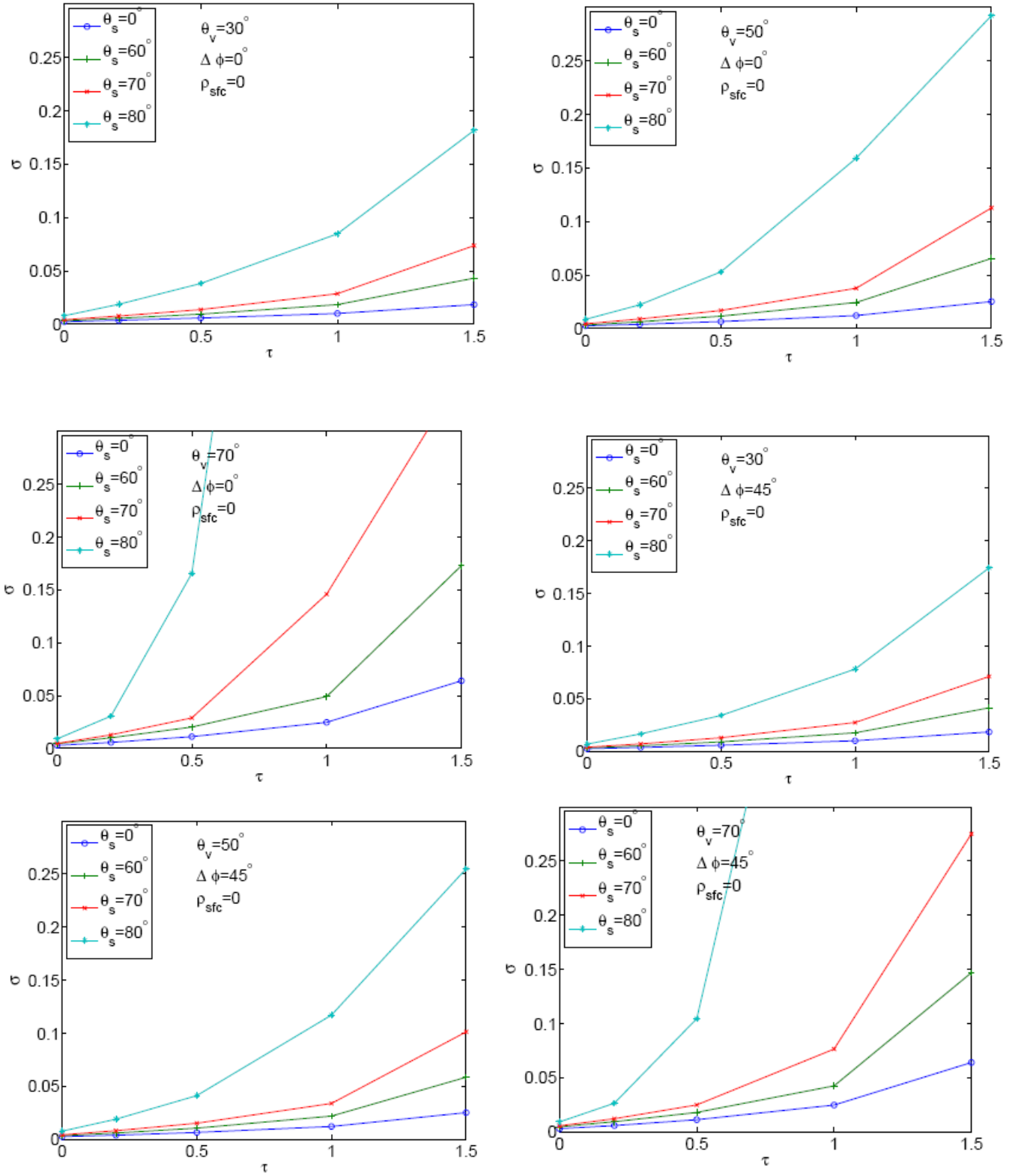
Figure 5: Standard deviation of AOD retrievals vs AOD for zero surface reflections.
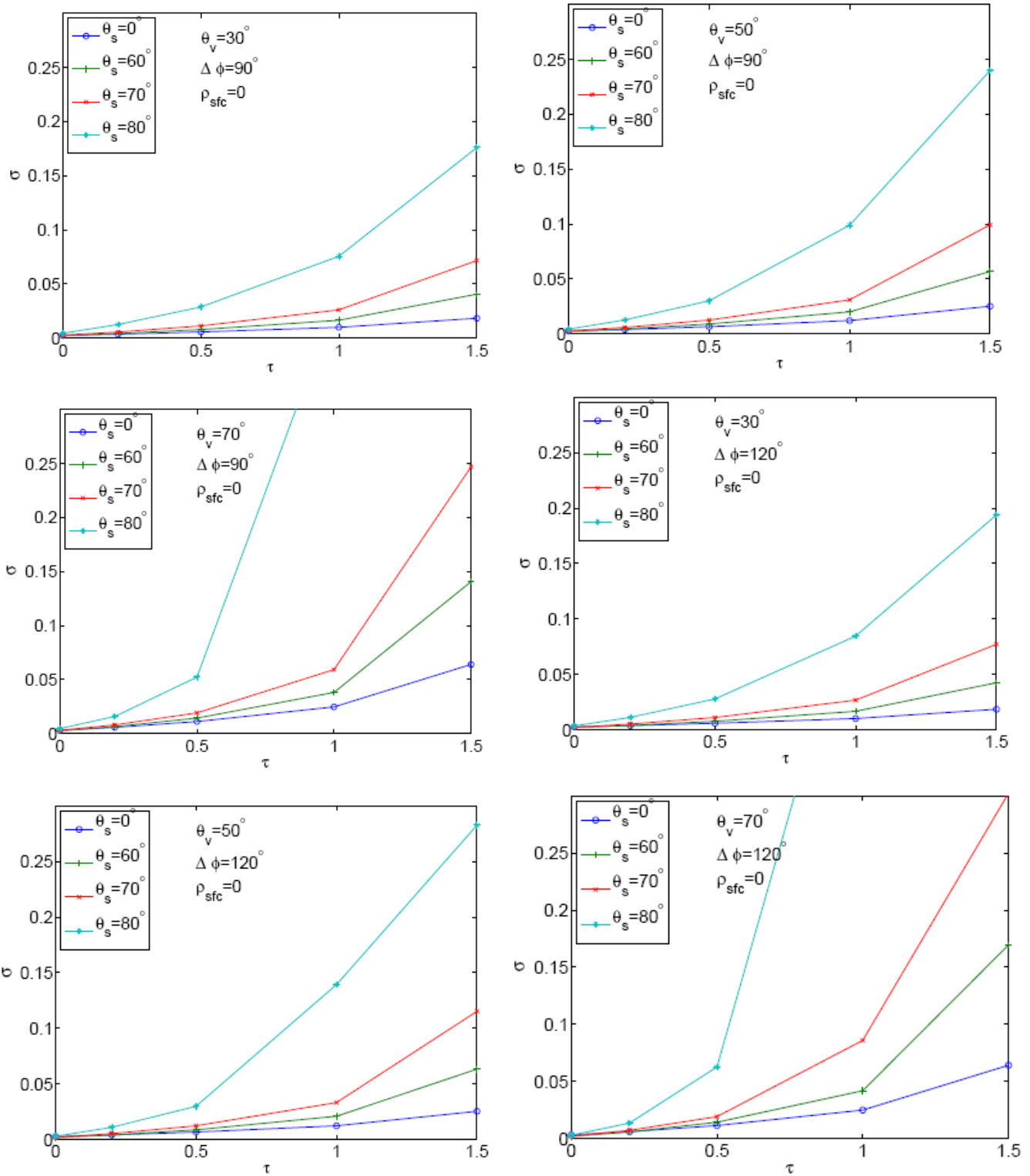
Figure 5: Standard deviation of AOD retrievals vs AOD for zero surface reflections (cont'd).
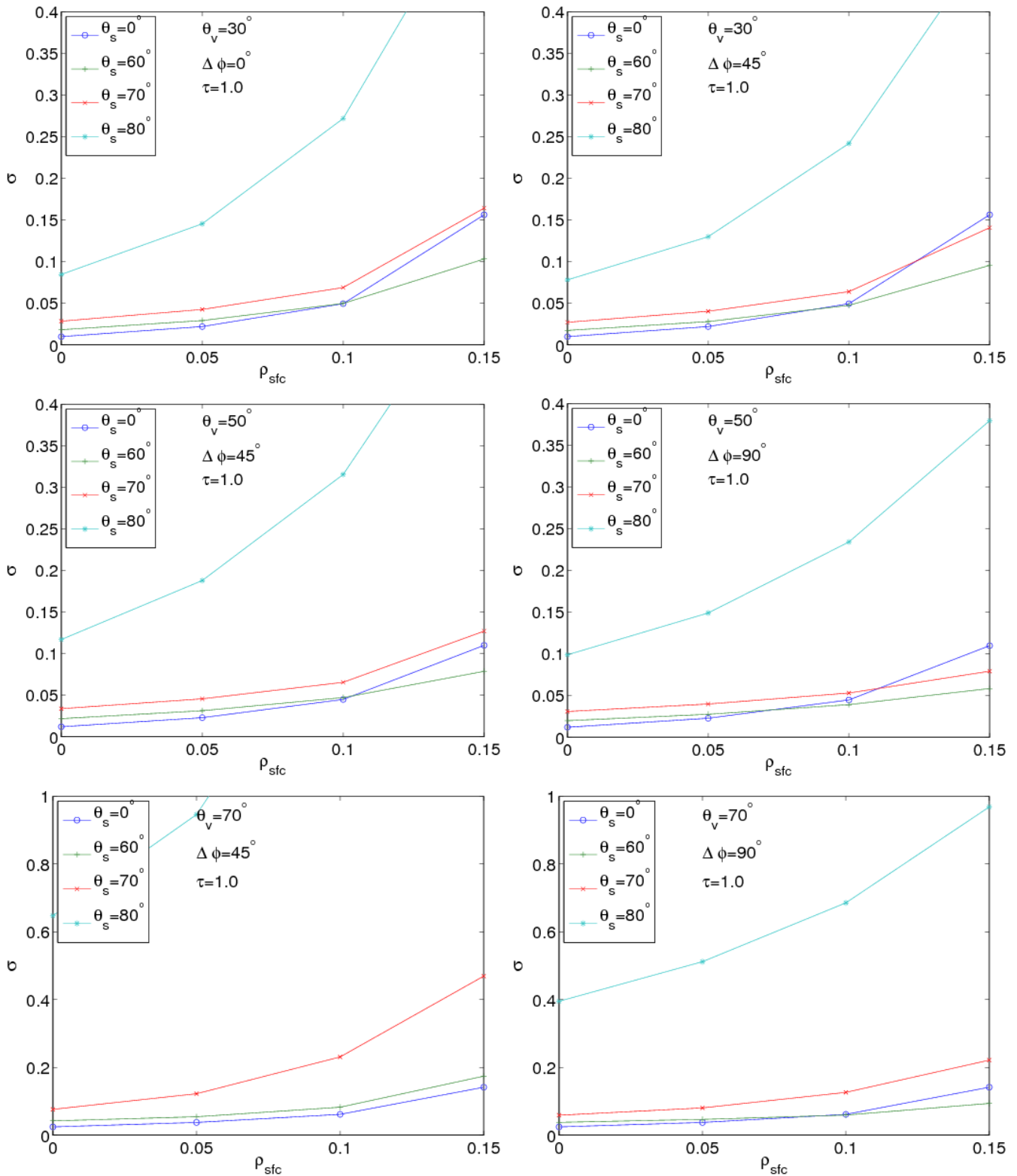
Figure 6: Standard deviation of AOD retrievals vs surface reflection for 1.0 AOD.

GOES 12 is located at 75˚W over the equator, and Figure 7 shows the zenith angle of the satellite at different locations over the US. The satellite zenith angle ranges from 30˚ at the southeast to 70˚ at the northwest. Figure 8 illustrate the solar zenith angle and the relative azimuth angle on January 1 and July 1. In the early morning and late in the afternoon when the sun just rises with large solar zenith angle greater

than 70˚, the uncertainties are expected to be high. The uncertainties are expected to be higher in winter for the northern part of the United States than those in the other seasons due to the large solar zenith angles. Because of the large satellite zenith angle at the northwest United States, which is about 70˚, the uncertainties should be higher there. The uncertainties should also be higher in the western United States than those in the eastern United States because the higher surface reflectance in the west.
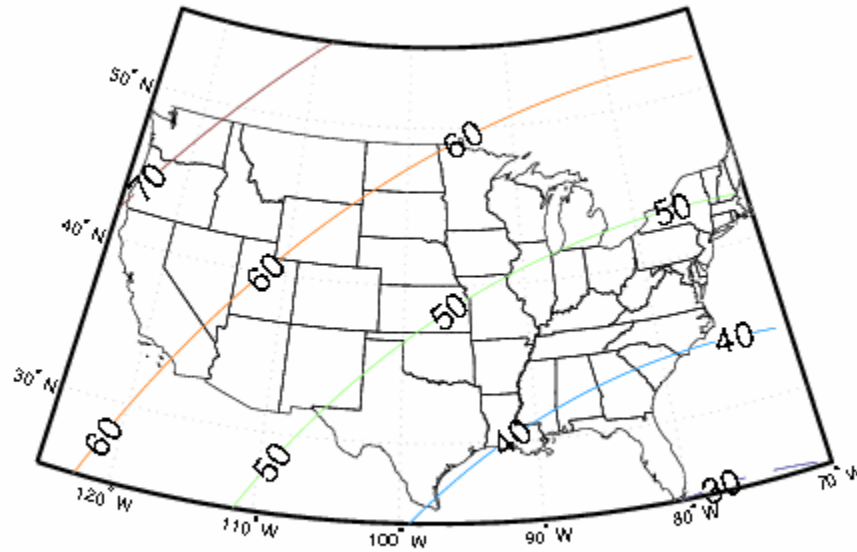

Figure 7: Satellite zenith angle (θ_v).
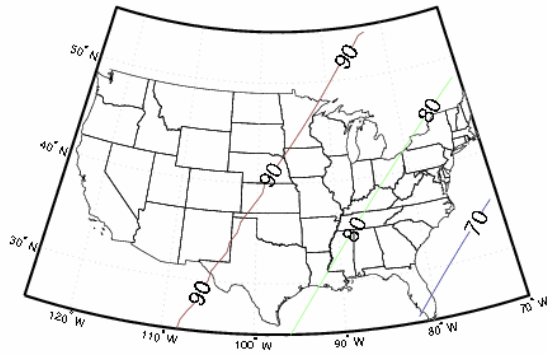
(a) θ_s at 1400 UTC on Jan,1.
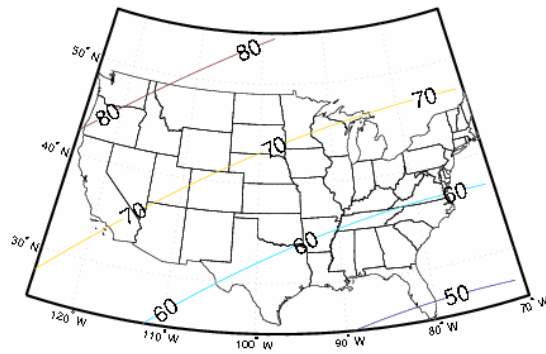
(b) θ_s at 1700 UTC on Jan,1.
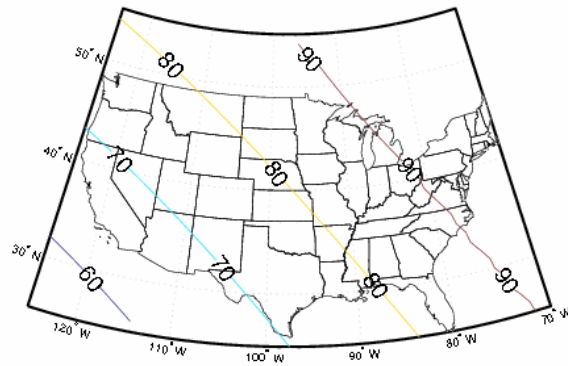
(c) θ_s at 2200 UTC on Jan,1.
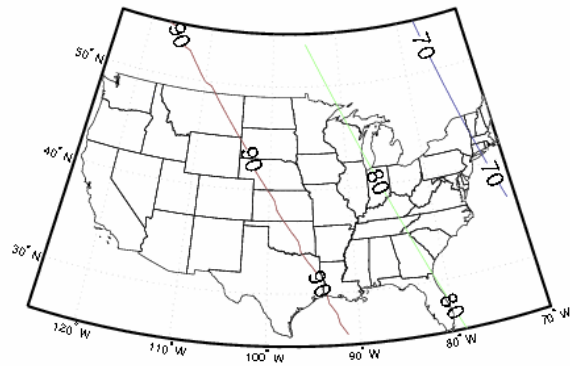
(d) θ_s at 1130 UTC on July,1.
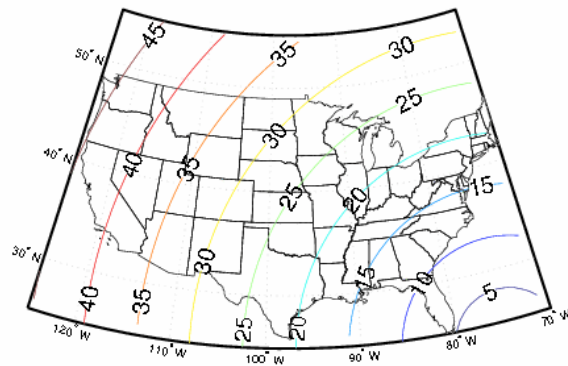
(e) θ_s at 1700 UTC on July,1.
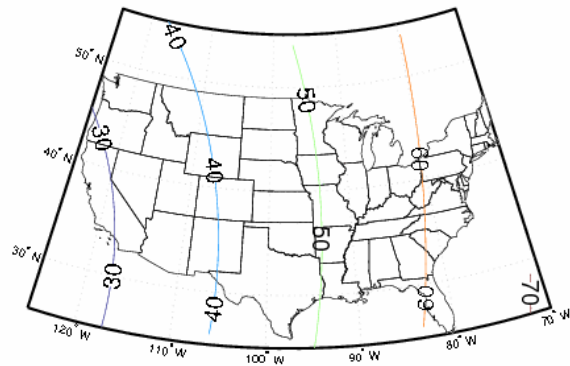
(d) θ_s at 2200 UTC on July,1.

Figure 8: Solar zenith angle (θ_s) on Jan,1 and July 1.

4.2. RETRIEVAL TESTS WITH REAL DATA

The LUT used in GASP is calculated by the 6S radiative transfer model, which accounts for the atmospheric effects including aerosol extinction, Rayleigh scattering and gaseous absorption. In order to estimate the errors caused by assuming a fixed value of the column water vapor and ozone, we perturb the column water vapor and ozone by making new LUTs with different concentrations. Two example LUTs are the ones made using extreme values: one using the minimum column water vapor and ozone and the other using the maximum. For the first LUT, which has the lowest gaseous absorption, the column water vapor is set to 0, and the column ozone is set to 220 DU. For the second one, which has the highest gaseous absorption, the column water vapor is set to 6 g cm^{-2}, and the column ozone is set to 450 DU. If we apply these two new LUTs to the GASP retrieval algorithms respectively, the differences between the AOD retrieved from the new LUTs and those from the original LUT are the maximum errors from the gaseous absorption. The average difference between the low-absorption reflectance and the original reflectance at TOA is around 6.0%, and the average difference between the high-absorption reflectance and the original reflectance is around -4.4%.

The effect of water vapor and ozone on the AOD retrieved is simulated through the retrieval cases on August 1, 2006, which include retrievals for every 30-minute timestep from 12:15 UTC to 22:15 UTC. The AOD retrieved with the original LUT at 14:45 UTC on this day is shown in Fig. 9. High AOD retrievals about 1.0 are observed on the east coast of the United States on this day.
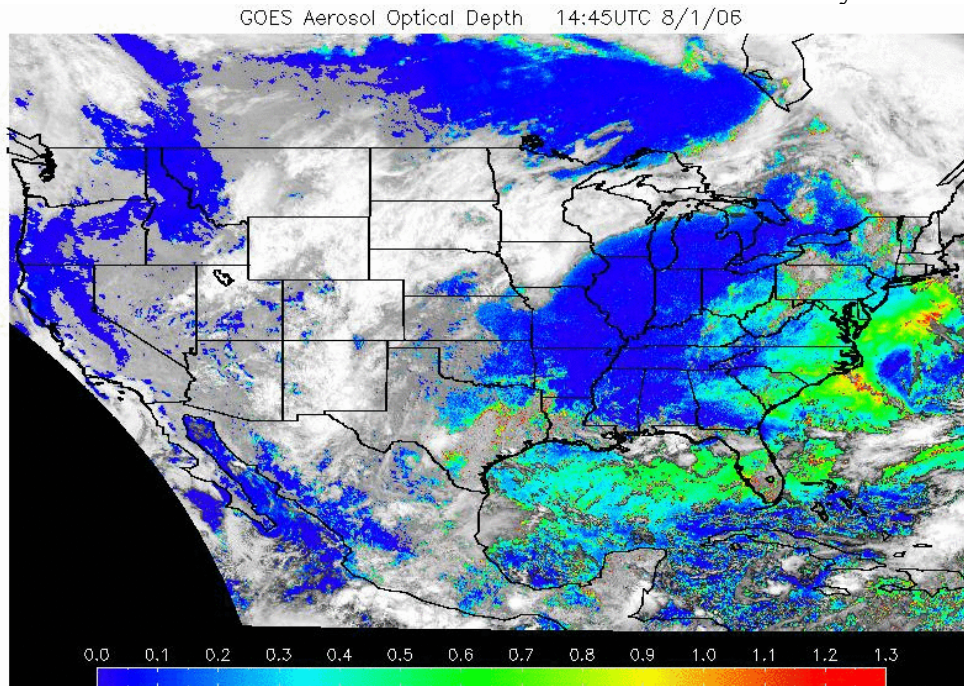
Figure 9: GOES AOD retrieved using original LUT on 8/1/2006 at 14:45 UTC (AOD$_0$).

To estimate the bound of the errors, the LUTs generated with two extreme absorptions are used for the retrieval. The effects are observed on the retrieval of surface reflectance, the retrieval of AOD, and the screening process.

Fig. 10 shows the scatter diagram for the retrieved surface reflectance using the new LUTs and original LUT for the 8/1/2006 14:45UTC case. As expected, the retrieved surface reflectance is lower using the low-absorptive LUT (ρ_{sfc1}) compared with that retrieved using original LUT (ρ_{sfc0}), and is higher with the high-absorptive LUT (ρ_{sfc2}). The difference between the ρ_{sfc1} and ρ_{sfc0} is about -5%, with a bias of -0.0039 and RMS 0.0049, while the difference between ρ_{sfc2} and ρ_{sfc0} is about 5%, with a bias of 0.0038 and RMS 0.0047.

Figure 10: Scatter diagram of the surface reflectance retrieved using new LUTs with different ozone and water vapor content. ρ_{sfc0} **is the surfa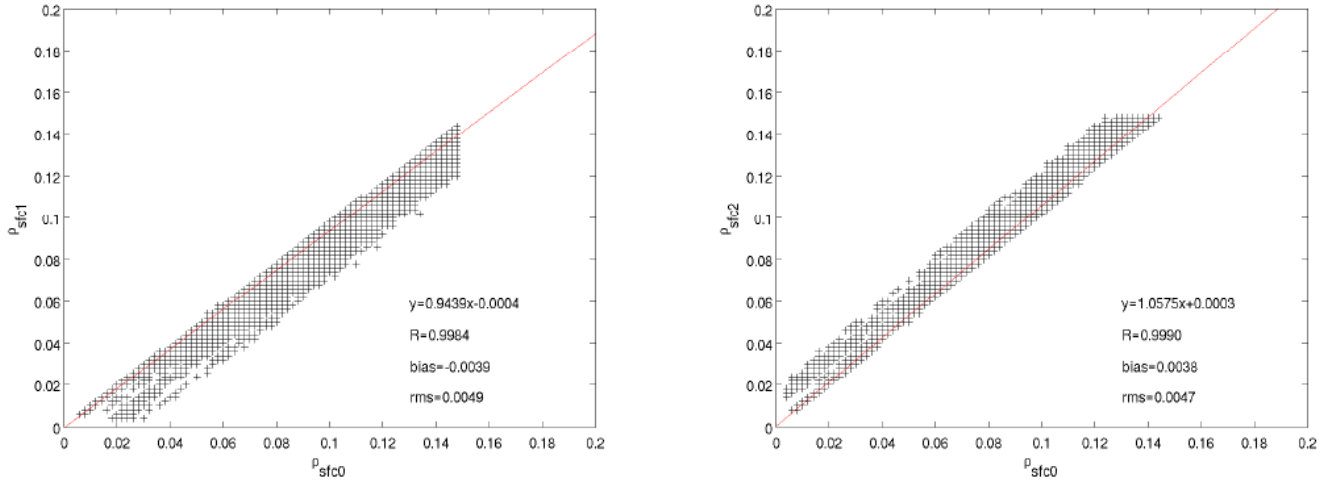ce reflectance retrieved with original LUT.** ρ_{sfc1} **is the surface reflectance retrieved with LUT computed with low concentration of ozone (220 DU) and water vapor (0 g cm^{-2}).** ρ_{sfc2} **is the surface reflectance retrieved with LUT computed with high concentration of ozone (450 DU) and water vapor (6 g cm−2).**

Fig. 11 shows the variation of slopes as a function of the time of during the day from 12:15 UTC to 22:15 UTC at 30-minute intervals. Large slope deviations are found in the early morning at 12:15 UTC due to the effect of the large solar zenith angle. During midday, i.e. from 14:15 UTC to 22:15 UTC, the slopes are nearly constant. The impact of the different gaseous absorption to the retrieved AOD is shown in Fig. 12, Fig.13, and Fig. 14 for August 1, 2006 at 14:45 UTC using different LUTs. Fig. 12 shows the scatter diagram between AODs retrieved. Fig. 13 shows the retrieved AOD maps with the new LUTs. Fig.14 shows the maps of AOD differences. As we can see, if the LUT with low concentration of water vapor and ozone is used, the retrieved AOD are smaller, and the retrieved AOD are larger if the LUT with high concentration is used. For the LUT generated with low extreme of absorptive gas (water vapor 0 and ozone 220 DU), the retrieved AOD (AOD$_1$ hereafter) produces a slope of 0.94, a bias of -0.016, and an RMS difference of 0.023 with the AOD using the original LUT (AOD$_0$ hereafter). For the LUT generated with high extreme of absorptive gas (water vapor 6 g cm^{-2} and ozone 450 DU), the retrieved AOD (AOD$_2$ hereafter) produces a slope of 1.04, a bias of 0.011, and an RMS difference of 0.016 with the AOD$_0$.
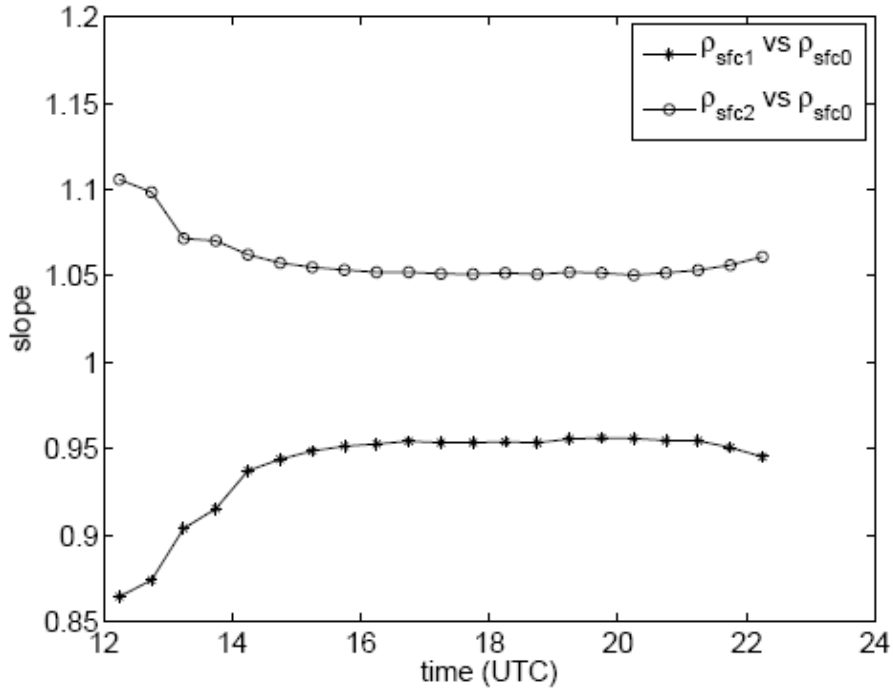
Figure 11: ρ_{sfc1} **vs** ρ_{sfc0} **slope and** ρ_{sfc2} **vs** ρ_{sfc0} **slope as a function of UTC time.**
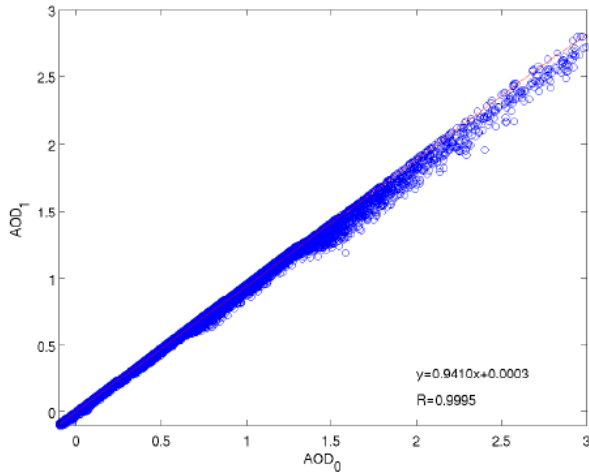
(a) AOD_0 vs AOD_1. RMS=0.023. N=611211.
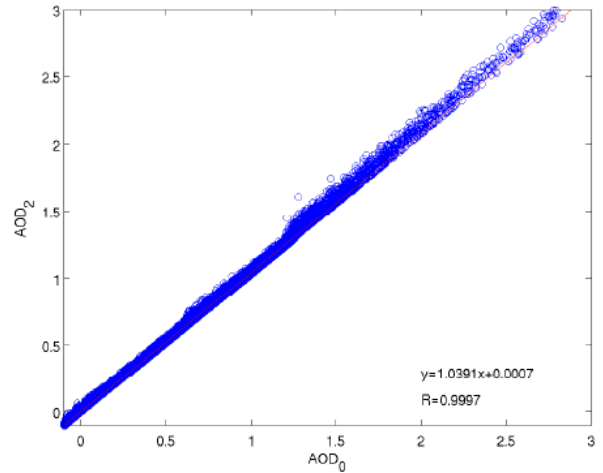
(b) AOD_0 vs AOD_2. RMS=0.016. N=598239.

Figure 12: Scatter diagram of the GOES AOD retrieved with different ozone and water vapor content. AOD_0 is the AOD retrieved with original LUT. AOD_1 is the AOD retrieved with LUT computed with low concentration of ozone (220 DU) and water vapor (0). AOD_2 is the AOD retrieved with LUT computed with high concentration of ozone (450 DU) and water vapor (6 g cm^{-2}). Of the three, AOD_1 has the most retrievals: 6.30 × 10^5 points in the frame of 2000 × 850. AOD_2 has the least: 5.98 × 10^5. AOD_0 is in between: 6.12 × 10^5.
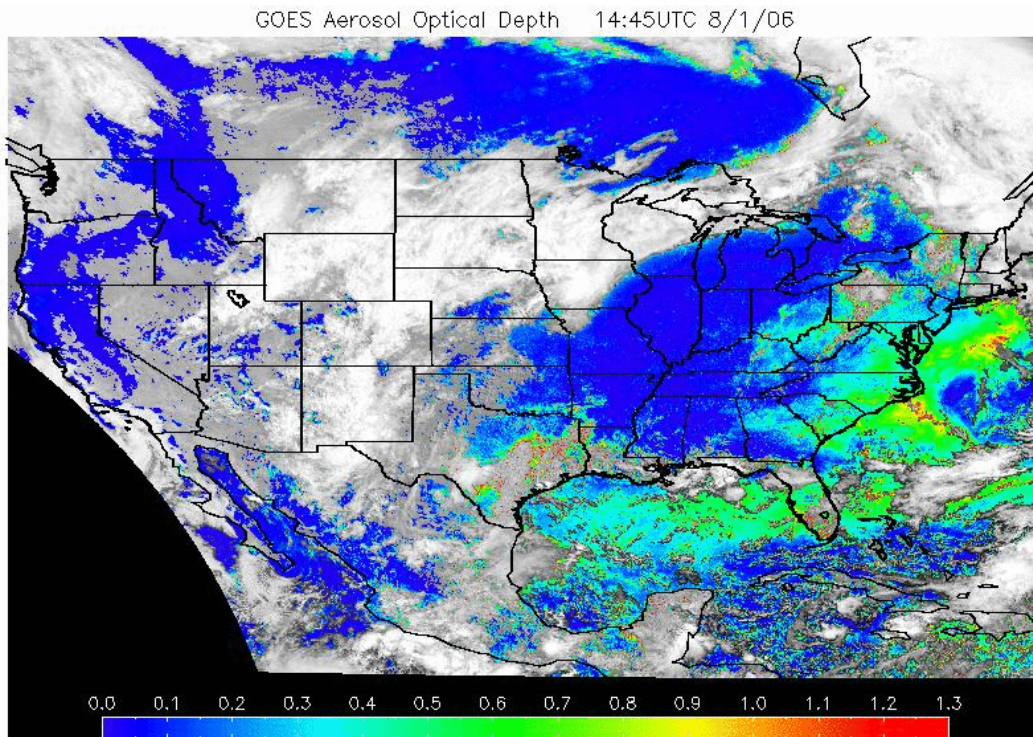
(a) AOD retrieval with low gaseous absorption LUT.
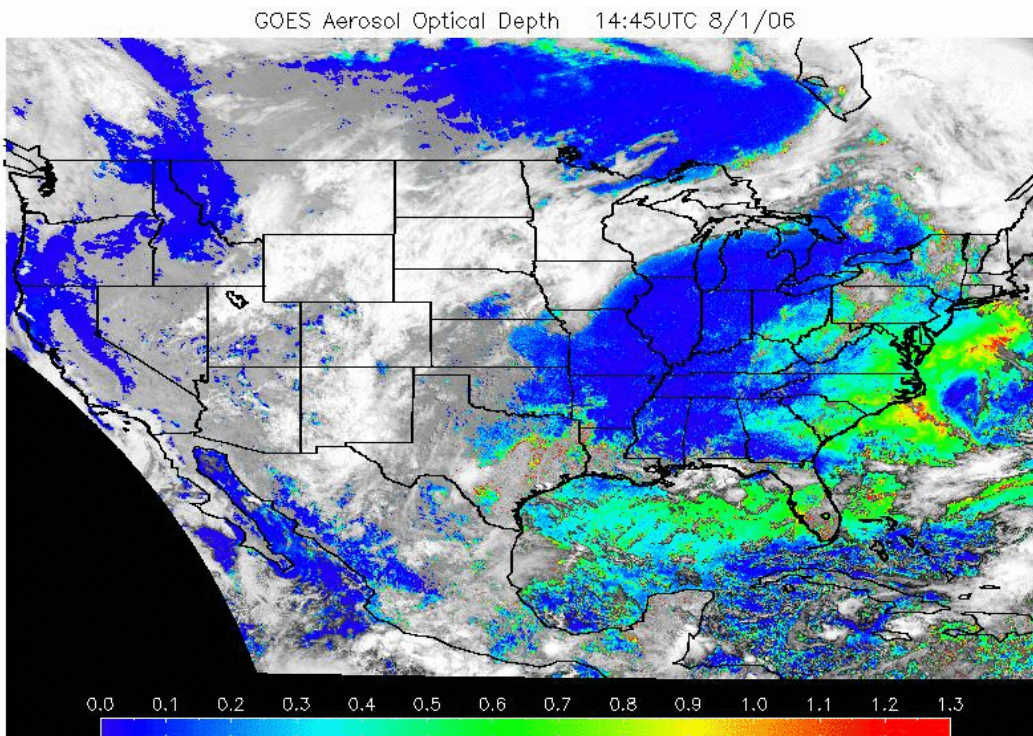
(b) AOD retrieval with high gaseous absorption LUT.

Figure 13: GOES AOD retrieved with different LUT for 8/1/2006 14:45 UTC.

16
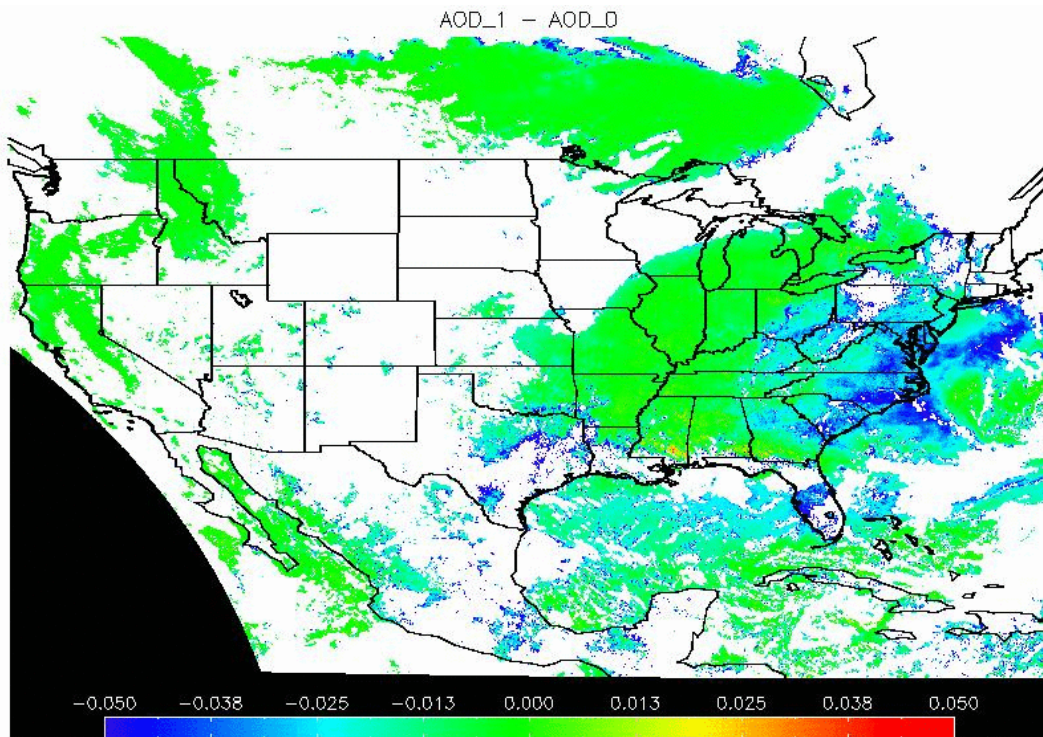
(a) $AOD_1 - AOD_0$
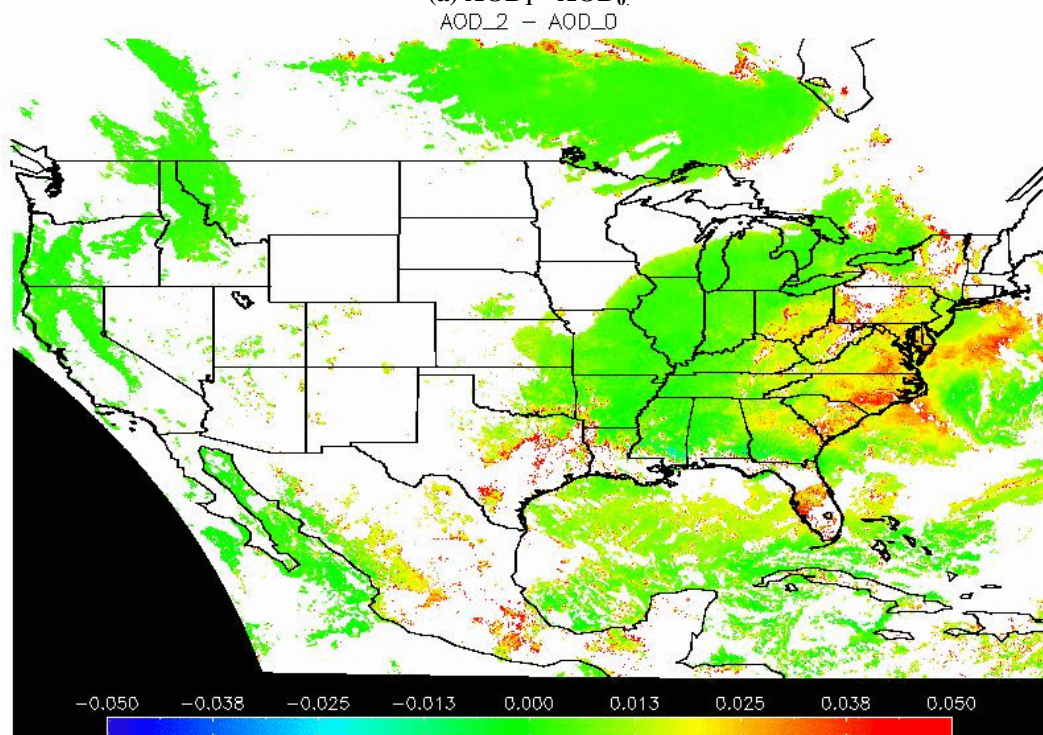
(b) $AOD_2 - AOD_0$
Figure 14: Difference in retrieved AOD with different LUTs.

Figure 15: AOD slope as a function of time.

The change of gaseous absorption also have some effect the screening scheme: low gaseous absorption LUT has more AOD retrievals. In the frame of 2000×850, AOD_1 has the largest number of retrievals with 6.30×10^5 pixels, AOD_2 has the least: 5.98×10^5, and AOD_0 is in between: 6.12×10^5. The differences are mostly located on the AOD map in Canada to the north of Montana and North Dakota, and in the states 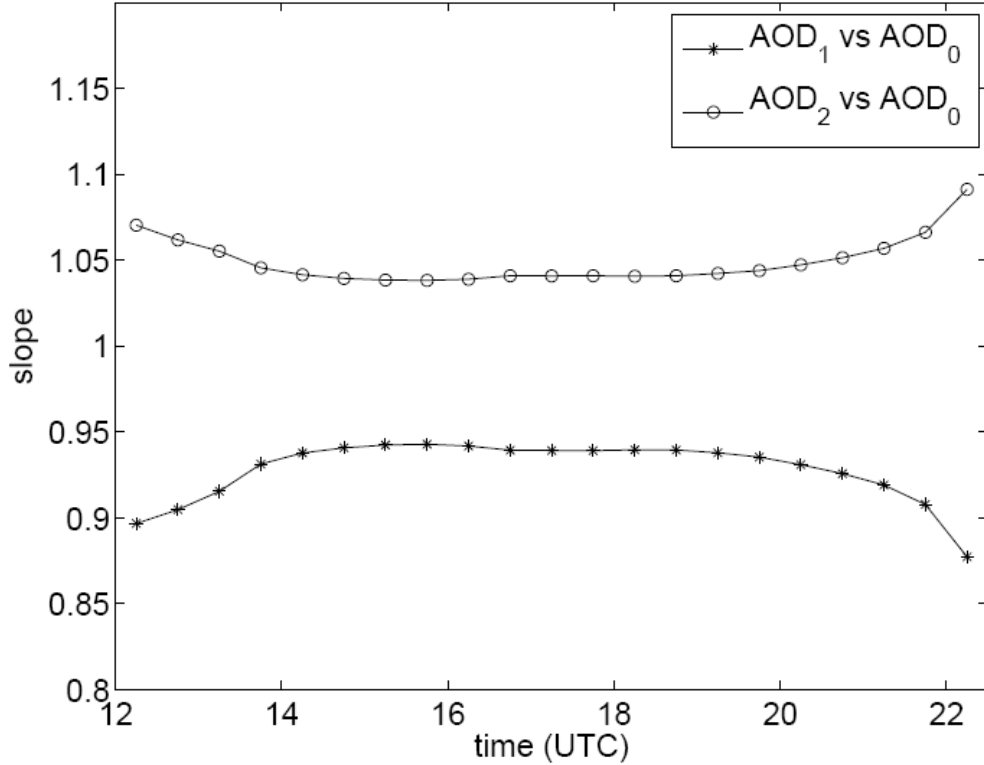of Nevada, Oregon and northern California. These pixels either have a standard deviation close to 0.3 within 3×3 pixel box or have a high surface reflectance close to 0.15.

The diurnal factors in the sun-satellite angles affect the LUT differences. Large differences are observed early in the morning and late in the afternoon when the zenith angle of the sun is large. Fig. 15 shows the slope as a function of time on August 1, 2006. The slopes are nearly constant during midday from 14:00 to 20:00 UTC, while the slopes in the early morning and in the late afternoon are different considerably from the midday values. The smallest slope for AOD_1 is about 0.85, and the largest slope for AOD_2 is about 1.10.

To estimate the influence on the slope by water vapor and ozone individually, we created four LUTs with the following column water vapor and ozone concentrations: 3.33 g cm^{-2} and 303 DU, 0.65 g cm^{-2} and 303 DU, 1.99 g cm^{-2} and 340 DU, 1.99 g cm^{-2} and 266 DU. By using these four LUTs in GASP, the tendency of the slope with respect to column water vapor and column ozone can be determined, i.e. $\partial A / \partial U_{H_2O}$ and $\partial A / \partial U_{O_3}$, where A is the slope, U_{H_2O} is column water vapor, and U_{O_3} is column ozone. $\partial A / \partial U_{H_2O}$ ranges from 0.0077 cm^2 g^{-1} to 0.021 cm^2 g^{-1} with small values in the mid-day and large values in the early morning and in the late afternoon. Similarly, $\partial A / \partial U_{O_3}$ ranges from 0.00027 DU^{-1} to 0.00097 DU^{-1}. From above calculation, the seasonal variation of mean column water vapor 1.79 g cm^{-2} can introduce a change of the slope between 0.014 and 0.038; the mean diurnal variation of column water vapor 0.66 g cm^{-2} can introduce a change of the slope between 0.0051 to 0.014; the seasonal variation of

mean column ozone 40 DU can introduce a change of the slope between 0.011 and 0.039; the mean diurnal variation of column ozone 30 DU can introduce change of the slope between 0.0081 to 0.029.

5. CORRECTION ALGORITHM

One solution to remove this error is to add two new dimensions in the LUT, i.e. ozone and water vapor, and to include inputs of real time distribution of ozone and water vapor in the retrieval algorithm. However, this may introduce more complication and computing resources especially in determining the surface reflectance. One would have to additionally compute the impact on the clear composite reflectance which is used as a reference and since these values arise from different days, the amounts of water vapor and ozone on those different pixels would not be uniform. This difficulty can be solved by switching the first and second step of the GASP retrieval algorithm. In the first step of the correction algorithm, we retrieve the reflectance with an assumption of 0.02 AOD for the previous 21 days. Then these reflectance maps are used to derive the surface reflectance in the second step such that the second darkest pixels are selected over the 21-day period.

We ran the correction algorithm for the retrievals in August 2006 and compared it with 10 AERONET stations over the eastern United States. The results are shown in Figure 16 and Figure 17, where the results from the same algorithm using the fixed values of column water vapor and ozone used in the original GASP algorithm are also shown for comparison. As we can see from these results, the differences between these two retrievals are very small: 0.01 in slope and correlation coefficient, less than 0.01 RMS errors.
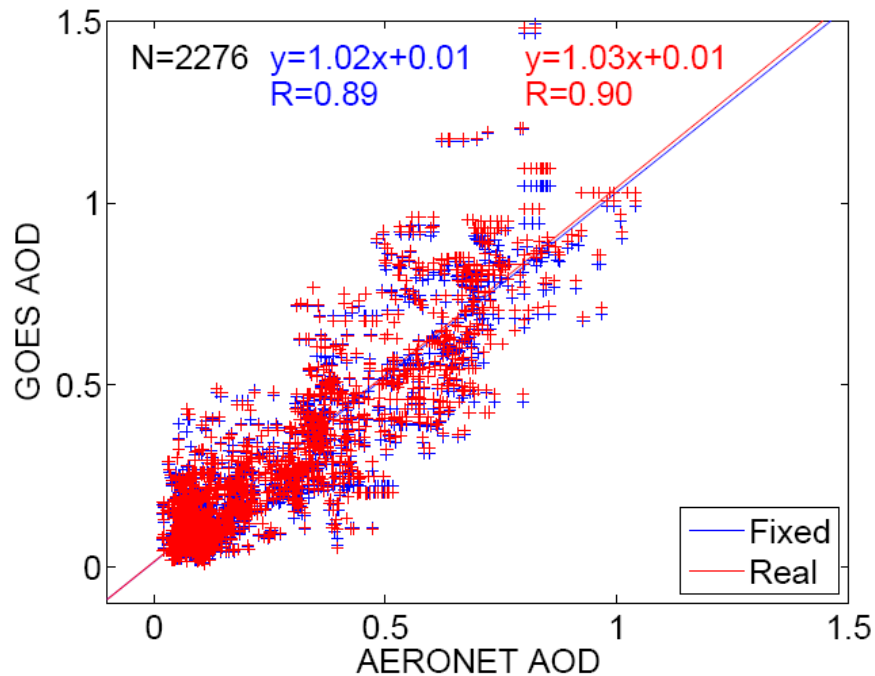

Figure 16: Comparison of the AOD retrievals corrected GASP algorithm with real water vapor and ozone and those with fixed values.
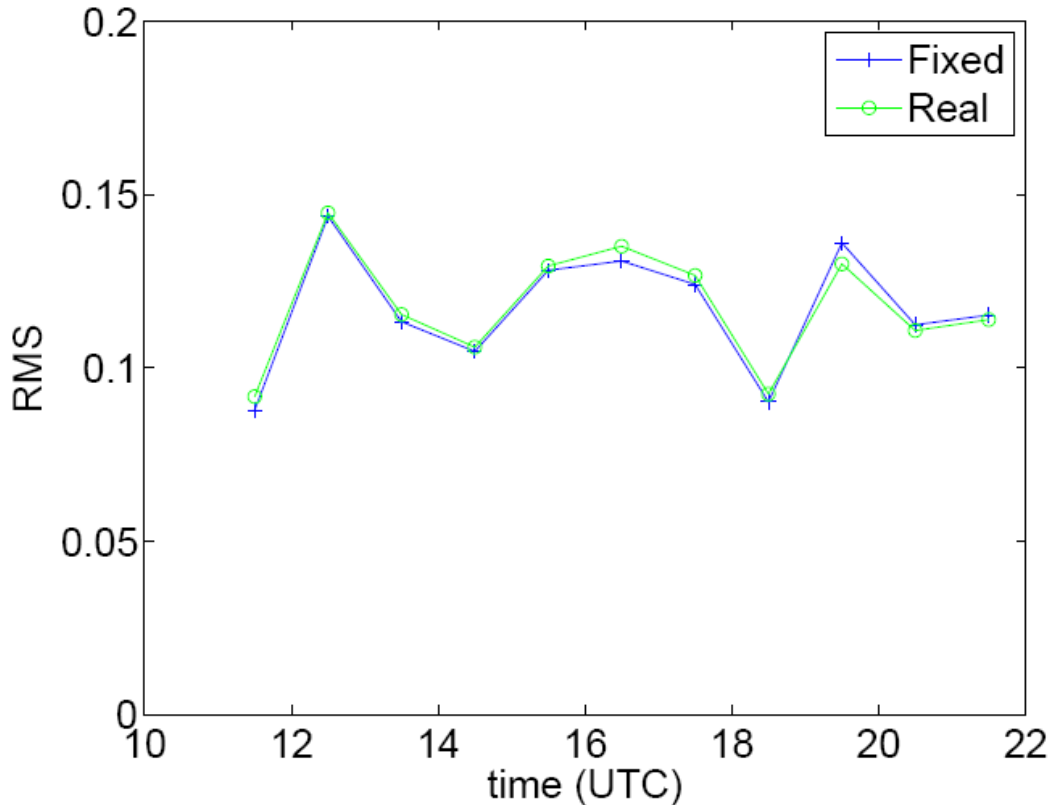
Figure 17: RMS error as a function of UTC time of the AOD retrievals corrected GASP algorithm with real water vapor and ozone and those with fixed values.

6. CONCLUSIONS
In this report, we performed tests for estimating the errors introduced by the ozone and water vapor content in the GASP retrieval. We found that the errors introduced by the water vapor and ozone are small in the small solar and satellite zenith angles: the uncertainties are less than 5% for solar zenith angle and satellite zenith angle less than 70˚. In the retrieval test using real data with two extreme cases, we found a mean difference -0.016(0.011), an RMS difference 0.023(0.016) and a slope 0.94(1.04) between the AOD retrieved with low(high)-absorption LUT and that from original LUT in midday, while in the early morning and in the late afternoon when the sun zenith angle is large, the slope is 0.85(1.10) for the retrieval from low(high)-absorption LUT. The average seasonal variation and average daily variation is much smaller than the above two extremes. This is a small error compared to the results of 20% error between GASP and AERONET (*Prados et al.* 2007).

Although large errors may occur in the extreme cases with large solar and satellite zenith angles, these cases do not often occur in real retrievals. A correction algorithm was introduced, and the results also show very small difference between the retrievals using real values of water vapor and ozone and fixed values. Based on our tests, we got the same conclusion as (*Knapp et al.* 2002) such that the current treatment of water vapor and ozone in GASP algorithm is satisfactory.

BIBLIOGRAPHY

Al-Saadi, J., et al. (2005), Improving national air quality forecasts with satellite aerosol observations, *Bul. of Amer. Meteor. Soc.*, *86*, 1249–1261.

Charlson, R., J. Langner, H. Rodhe, C. Leovy, and S. Warren (1991), Perturbation of the northern hemisphere radiative balance by backscattering from anthropogenic sulfate aerosols, *Tellus*, *43(4)*, *152–163* doi:10.1034/j.1600-0889.

Engel-Cox, J., C. Holloman, B. Coutant, and R. Hoff (2004), Qualitative and quantitative evaluation of MODIS satellite sensor data for regional and urban scale air quality, *Atmos. Environ.*, *38*, 2495–2509.

Haywood, J., V. Ramaswamy, and B. Soden (1999), Tropospheric aerosol climate forcing in clear sky satellite observations over the oceans, *Science*, *283*, 1299–1303.

Herman, B., and S. Browning (1975), The effect of aerosols on the earth-atmosphere albedo, *J.Atmos.Sci.*, *32*, 1430–1445.

Hoff, R., S. Palm, J. Engel-Cox, and J. Spinhirne (2005), GLAS long-range transport observation of 2003 California forest fire plumes to the northeastern US, *Geophys.Res.Lett.*, *32*, L22S08.

Kaufman, Y., J. Tanre, L. Remer, E. Vermote, A. Chu, and B. Holben (1997), Operational remote sensing of tropospheric aerosols over land from EOS moderate imaging spectro-radiometer, *J.Geophys. Res.*, *102(D14)*, 17,051–17,068.

Kaufman, Y., D. Tanre, and O. Boucher (2002), A satellite view of aerosols in the climate system, *Nature*, *419*, 215–223.

Knapp, K., and T. Vonder Haar (2000), Calibration of the eighth geostationary observational environmental satellite (GOES-8) imager visible sensor, *J.Atmos.Oceanic Tech.*, *17*, 1639–1644.

Knapp, K., T. Von der Haar, and Y. Kaufman (2002), Aerosol optical depth retrieval from GOES-8: uncertainty study and retrieval validation over South America, *J. Geophys. Res.*, *107(D7)*, 4055, doi:10.1029/2001JD00505.

Knapp, K., R. Frouin, S. Kondragunta, and A. Prados (2005), Toward aerosol optical depth retrievals over land from GOES visible radiances: determining surface reflectance, *Int. Journal of Remote Sensing*, *26*, 4097–4116.

Platnick, S., and S. Twomey (1994), Remote sensing the susceptibility of cloud albedo to changes in drop concentration, *Atmospheric Research*, *34*, 85–98.

Prados, A., S. Kondragunta, I. Laszlo, P. Ciren, and K. Knapp (2007), The GOES Aerosol/Smoke Product (GASP) over north america: Comparisons to AERONET and MODIS, *J. Geophys. Res.*, *112*, D15,201, doi:10.1029/2006JD007968.

Remer, L., et al. (2005), The MODIS Aerosol Algorithm, Products, and Validation., *J. of Atmos. Sci.*, *62*, 947–973.

Vermote, E., D. Tanre, J. Deuze, M. Herman, and J. Morcrette (1997), Second simulation of the satellite signal in the solar spectrum, 6S: An overview, *IEEE Trans. Geosci. Remote Sens.*, *35*, 675–686.

NESDIS 107   NOAA Operational Sounding Products for Advanced-TOVS: 2002.   Anthony L. Reale, Michael W. Chalfant, Americo S. Allergrino, Franklin H. Tilley, Michael P. Ferguson, and Michael E. Pettey, December 2002.

NESDIS 108   Analytic Formulas for the Aliasing of Sea Level Sampled by a Single Exact-Repeat Altimetric Satellite or a Coordinated Constellation of Satellites. Chang-Kou Tai, November 2002.

NESDIS 109   Description of the System to Nowcast Salinity, Temperature and Sea nettle (*Chrysaora quinquecirrha*) Presence in Chesapeake Bay Using the Curvilinear Hydrodynamics in3-Dimensions (CH3D) Model.   Zhen Li, Thomas F. Gross, and Christopher W. Brown, December 2002.

NESDIS 110   An Algorithm for Correction of Navigation Errors in AMSU-A Data. Seiichiro Kigawa and Michael P. Weinreb, December 2002.

NESDIS 111   An Algorithm for Correction of Lunar Contamination in AMSU-A Data. Seiichiro Kigawa and Tsan Mo, December 2002.

NESDIS 112   Sampling Errors of the Global Mean Sea Level Derived from Topex/Poseidon Altimetry. Chang-Kou Tai and Carl Wagner, December 2002.

NESDIS 113   Proceedings of the International GODAR Review Meeting: Abstracts. Sponsors: Intergovernmental Oceanographic Commission, U.S. National Oceanic and Atmospheric Administration, and the European Community, May 2003.

NESDIS 114   Satellite Rainfall Estimation Over South America: Evaluation of Two Major Events. Daniel A. Vila, Roderick A. Scofield, Robert J. Kuligowski, and J. Clay Davenport, May 2003.

NESDIS 115   Imager and Sounder Radiance and Product Validations for the GOES-12 Science Test. Donald W. Hillger, Timothy J. Schmit, and Jamie M. Daniels, September 2003.

NESDIS 116   Microwave Humidity Sounder Calibration Algorithm. Tsan Mo and Kenneth Jarva, October 2004.

NESDIS 117   Building Profile Plankton Databases for Climate and EcoSystem Research. Sydney Levitus, Satoshi Sato, Catherine Maillard, Nick Mikhailov, Pat Cadwell, Harry Dooley, June 2005.

NESDIS 118   Simultaneous Nadir Overpasses for NOAA-6 to NOAA-17 Satellites from 1980 and 2003 for the Intersatellite Calibration of Radiometers. Changyong Cao, Pubu Ciren, August 2005.

NESDIS 119   Calibration and Validation of NOAA 18 Instruments. Fuzhong Wang and Tsan Mo, December 2005.

NESDIS 120   The NOAA/NESDIS/ORA Windsat Calibration/Validation Collocation Database. Laurence Connor, February 2006.

NESDIS 121   Calibration of the Advanced Microwave Sounding Unit-A Radiometer for METOP-A. Tsan Mo, August 2006.

NESDIS 122   JCSDA Community Radiative Transfer Model (CRTM). Yong Han, Paul van Delst, Quanhua Liu, Fuzhong Weng, Banghua Yan, Russ Treadon, and John Derber, December 2005.

NESDIS 123   Comparing Two Sets of Noisy Measurements. Lawrence E. Flynn, April 2007.

NESDIS 124   Calibration of the Advanced Microwave Sounding Unit-A for NOAA-N'. Tsan Mo, September 2007.

NESDIS 125   The GOES-13 Science Test: Imager and Sounder Radiance and Product Validations. Donald W. Hillger, Timothy J. Schmit, September 2007

NESDIS 126   A QA/QC Manual of the Cooperative Summary of the Day Processing System. William E. Angel, January 2008.

NESDIS 127   The Easter Freeze of April 2007: A Climatological Perspective and Assessment of Impacts and Services. Ray Wolf, Jay Lawrimore, April 2008.

NOAA SCIENTIFIC AND TECHNICAL PUBLICATIONS

The National Oceanic and Atmospheric Administration was established as part of the Department of Commerce on October 3, 1970. The mission responsibilities of NOAA are to assess the socioeconomic impact of natural and technological changes in the environment and to monitor and predict the state of the solid Earth, the oceans and their living resources, the atmosphere, and the space environment of the Earth.

The major components of NOAA regularly produce various types of scientific and technical information in the following types of publications

PROFESSIONAL PAPERS – Important definitive research results, major techniques, and special investigations.

CONTRACT AND GRANT REPORTS – Reports prepared by contractors or grantees under NOAA sponsorship.

ATLAS – Presentation of analyzed data generally in the form of maps showing distribution of rainfall, chemical and physical conditions of oceans and atmosphere, distribution of fishes and marine mammals, ionospheric conditions, etc.

TECHNICAL SERVICE PUBLICATIONS – Reports containing data, observations, instructions, etc. A partial listing includes data serials; prediction and outlook periodicals; technical manuals, training papers, planning reports, and information serials; and miscellaneous technical publications.

TECHNICAL REPORTS – Journal quality with extensive details, mathematical developments, or data listings.

TECHNICAL MEMORANDUMS – Reports of preliminary, partial, or negative research or technology results, interim instructions, and the like.

U.S. DEPARTMENT OF COMMERCE
National Oceanic and Atmospheric Administration
National Environmental Satellite, Data, and Information Service
Washington, D.C. 20233